Clinical and Experimental Medicine (2025) 25:40
https://doi.org/10.1007/s10238-024-01526-6

RESEARCH

Enhancing staging in multiple myeloma using an m6A regulatory gene-pairing model

Yating Deng[1,2,3] · **Hongkai Zhu**[1,2,3] · **Hongling Peng**[1,2,3,4]

Received: 29 September 2024 / Accepted: 20 November 2024

Abstract

Multiple myeloma (MM) is characterized by clonal plasma cell proliferation in the bone marrow, challenging prognosis prediction. We developed a gene-pairing prognostic risk model using m6A regulatory genes and a nested LASSO method. A cutoff of − 0.133 categorized MM samples into high-risk and low-risk groups. The model showed strong prognostic performance in 2088 newly diagnosed MM samples and predicted response to combination therapy (daratumumab, carfilzomib, lenalidomide, and dexamethasone) in patients who failed or relapsed from bortezomib-containing regimens, with an AUC of 0.9. It distinguished between smoldering MM and MM (cutoff: − 0.45) and between MM and plasma cell leukemia (cutoff: 0.0857). Single-cell analysis revealed higher risk scores at relapse. Combining MM cell lines and sample data, we identified potential drugs and targets (ADAT2 and NUP153) effective against high-risk MM. Integrating the m6A risk model with the International Staging System (ISS) enhanced stratification accuracy. These insights support precision treatment of MM.

Graphical Abstract

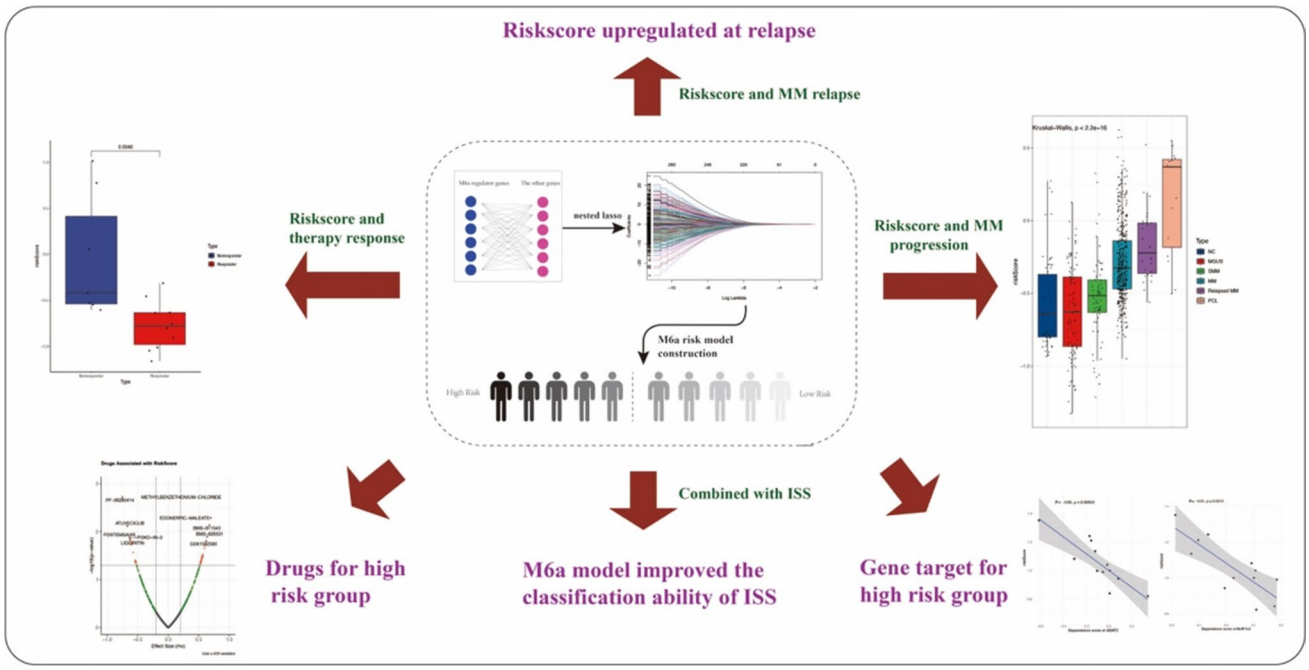

Keywords Multiple myeloma · Risk stratification · m6A

Extended author information available on the last page of the article

Published online: 17 January 2025

Introduction

Multiple myeloma (MM) is characterized by malignant monoclonal plasma cells in the bone marrow, with a global incidence of 6–7 per 100,000 humans annually [1, 2]. The progression of MM can be subdivided into several stages, including monoclonal gammopathy of undetermined significance (MGUS), smoldering myeloma (SMM), MM, and plasma cell leukemia (PCL). MGUS represents the initial stage, with approximately 1% of MGUS patients progressing to MM. The second stage, SMM, displays the same morphological characteristics as MM tumor cells but without significant organ damage, with about 10% of these cases transforming into MM [3]. Ultimately, MM tumor cells dissociate from the bone marrow microenvironment, progressing to PCL or extramedullary multiple myeloma (EMM) [4].

Identifying high-risk multiple myeloma (MM) patients is crucial for precision treatment. The International Staging System (ISS) [5] and Revised International Staging System (R-ISS) [6] are commonly used clinical methods for assessing poor prognosis in MM. The R-ISS incorporates abnormal karyotype data into the ISS, but these karyotypes are specific to certain treatment regimens and may lose their effectiveness with newer therapies. Risk models based on transcription levels can predict the prognosis of MM patients in real time with accuracy [7]. However, their major drawback is the lack of absolute quantifiability, as they are influenced by different measurement methods and batch effects, which compromises their clinical applicability. Gene-pairing models can effectively address these limitations of transcriptional models. Gene-pairing relies on comparing the expression level differences between two genes, significantly reducing batch effects and the impact of varying measurement methods. W. Kong and colleagues developed a gene-pairing model using pyroptosis-related genes to predict the prognosis of acute myeloid leukemia (AML) patients. Compared to non-pairing models, this approach significantly improved both accuracy and usability [8].

N6-methyladenosine (m6A) is the most common internal RNA modification in eukaryotic cells, influencing various aspects of RNA metabolism and playing a crucial role in the development and progression of multiple types of cancer. In multiple myeloma (MM), numerous studies have demonstrated the significant role of m6A in MM pathogenesis. HNRNPA2B1 promotes MM tumor cell proliferation by regulating ILF3-dependent AKT3 expression [9] and by enhancing cell proliferation through the TLR4 signaling pathway while regulating apoptosis [10]. FTO significantly promotes MM cell proliferation, migration, and invasion by targeting HSF1/HSPs in a YTHDF2-dependent manner [11]. IDH2 regulates global m6A RNA modification in MM by targeting the RNA demethylase FTO. The imbalance of m6A methylation enhances the expression of WNT7B, activating the Wnt signaling pathway and thus promoting MM tumorigenesis and progression [12]. High expression of YTHDF2 promotes MM cell proliferation through the EGR1/p21cip1/waf1/CDK2-cyclin E1 axis-mediated cell cycle transition [13]. In another study, both in vitro and in vivo experiments demonstrated that reducing YTHDF2 expression inhibited MM cell proliferation, while enforced expression of YTHDF2 reversed these effects. m6A-RIP sequencing and RIP-PCR analyses identified STAT5A as a downstream target of YTHDF2, with YTHDF2 promoting the degradation of STAT5A mRNA by binding to its m6A modification sites [14]. The METTL3/YY1/miR-27a-3p axis influences MM cell growth, apoptosis, and stem cell properties in both in vitro and in vivo settings [15]. Research has shown that ALKBH5 is highly expressed in primary CD138 + plasma cells isolated from MM patients and in MM cell lines. Reducing ALKBH5 expression inhibits the proliferation, angiogenesis, invasion, and migration of myeloma cells, while promoting apoptosis both in vitro and in vivo [16].

This study culminates in the creation of a novel gene-pairing-based prognostic model, utilizing an aggregated m6A regulatory gene repository. We have demonstrated that the model possesses excellent risk prediction performance and clinical applicability. By integrating it with the ISS, we developed an m6A-refined ISS, significantly enhancing the risk stratification capabilities of the ISS. Furthermore, the m6A model's risk scores are strongly associated with MM disease progression and the development of drug resistance.

Methods

Data collection

For the construction of the m6A signature, we utilized gene expression profiles of CD138 + selected plasma cells along with clinical information from five multiple myeloma (MM) cohorts, encompassing a total of 2080 MM patients. The datasets were primarily sourced from the Gene Expression Omnibus (GEO) database and The Cancer Genome Atlas (TCGA) database. For detailed information, please refer to Supplementary Table 1. Twenty-seven m6A regulatory genes were identified from currently published literature [17–20] and are listed in Supplementary Table 2. Gene expression data for different stages of MM progression (normal control, MGUS, SMM, newly diagnosed MM, relapsed MM, and PCT) were obtained from seven GEO datasets, including GSE13591, GSE16558, GSE2113, GSE39754, GSE47552, GSE5900, and GSE6477. Specific information

is provided in Supplementary Table 3. Additionally, the single-cell sequencing data were obtained from GSE161195 [21] and GSE193695 [22] (Supplementary Table 4). The PRISM Repurposing Public 23Q2 drug sensitivity data and the combined RNAi dependency score data for MM cell lines were obtained from the DepMap portal (https://depmap.org/portal/)(23).

Construction and validation of a m6A risk score

We leveraged the MMRF-CoMMpass dataset, the largest cohort in our study (n = 796), to develop a training set. Two-thirds of these samples were randomly selected for model training, while the remaining one-third were reserved for internal validation. External validation was conducted using the GSE24080, GSE136337, GSE57317, and GSE19784 datasets. In the training cohort, we utilized univariate Cox regression and Kaplan–Meier (KM) survival analysis to identify m6A-related genes significantly associated with multiple myeloma (MM) prognosis. Patients were divided into two groups for KM curve analysis based on an optimal cutoff value. Genes with a p-value less than 0.05 in either the Cox or KM analysis were selected for further evaluation, resulting in the identification of 13 m6A regulatory genes that met these criteria.

Next, we paired the 13 m6A regulatory genes with other available genes and employed a nested LASSO method [24] to construct a gene-paired prognostic model. The gene-pair value was determined by comparing the expression levels of two genes. For instance, if gene A had higher expression than gene B, it was denoted as A|B = 1; otherwise, it was denoted as A|B = -1. After excluding gene-pairs with low variability and those not related to prognosis, further selection was performed using LASSO regression. The detailed methodology is illustrated in Supplementary Fig. 1. After constructing the model, we calculated a risk score for each multiple myeloma (MM) sample using the linear formula: RiskScore = ∑(coef*GenePAIR). In the training cohort, we utilized the 'surv_cutpoint' function from the 'survminer' package to determine the optimal cutoff value, which maximized the survival difference between high-risk and low-risk groups. This cutoff value was then uniformly applied to the validation cohorts for risk stratification.

The accuracy evaluation of the m6A risk score in predicting the therapy response for MM treatment

In the GSE161195 dataset, which includes baseline single-cell transcriptome data of refractory MM patients who received a bortezomib-based induction, these patients subsequently underwent a DARA-KRD regimen (daratumumab, carfilzomib, lenalidomide, and dexamethasone). Among the 34 MM patients with baseline single-cell transcriptome data, therapy response has been recorded for 17 of them.

For the single-cell transcriptome data, quality control and normalization steps were performed as described in the original article [21] using the Seurat package. The count data from cells corresponding to each sample were aggregated into pseudobulk count data using the 'AggregateExpression' function. Subsequently, we calculated the risk score for each sample in the same manner as for the bulk RNA-seq samples.

We compared and visualized the risk scores between the responder and non-responder groups using boxplots created with the 'ggplot2' package. Additionally, we generated an ROC plot using the 'pROC' package to evaluate the ability of the risk score to distinguish between different response groups.

Variation of m6A risk scores across different stages of multiple myeloma progression

Multiple myeloma (MM) can be classified into various stages of disease progression, including monoclonal gammopathy of undetermined significance (MGUS), smoldering multiple myeloma (SMM), newly diagnosed MM, relapsed MM, and plasma cell leukemia (PCL). We collected gene expression data from multiple GEO datasets containing samples from these different stages. Given that the gene-pairing model significantly enhances comparability across different batches of data, we merged multiple array datasets and calculated the m6A risk score for each sample in the combined array. The Kruskal–Wallis test was used to analyze the significance of differences among groups. Additionally, we assessed the ability of the risk scores to distinguish between any two disease stages using the area under the curve (AUC) metric, with the 'pROC' package employed for these analyses.

Measuring the change in risk score from initial diagnosis to relapse

In Sect. "Variation of m6A risk scores across different stages of multiple myeloma progression," we have already examined the difference in risk scores between initial diagnosis MM and relapse MM samples, but this was not done using paired samples. The GSE193695 dataset contains single-cell transcriptome data for a Japanese MM patient, with samples spanning four time points: initial diagnosis (p1), relapse after lenalidomide treatment (p3), relapse after lenalidomide and ixazomib treatment (p4), and relapse after daratumumab and bortezomib treatment (p5). Additionally, the GSE161195 dataset includes single-cell data from paired samples for the same MM patient who underwent the DARA-KRD regimen,

with time points spanning from baseline to after cycles 4 and 10 of therapy.

For the single-cell data, we performed quality control and data normalization using the Seurat package, following the methodology described in the original paper. In the analysis of the GSE193695 dataset, we first calculated the risk score for each cell using the normalized data and then compared the risk scores across different time points. For the GSE161195 dataset, we generated pseudobulk data for each sample and calculated the risk score for each sample as described in Sect. "The accuracy evaluation of the m6A risk score in predicting the therapy response for MM treatment." Subsequently, we conducted pair-wise comparisons of the risk scores among the baseline, cycle 4, and cycle 10 time points.

Screening drugs and targets for high-risk score multiple myeloma (MM)

The PRISM Repurposing Public 23Q2 drug sensitivity data [25] were downloaded from the DepMap website. This dataset contains cell viability fold change measurements at a 2.5 μM concentration for various drugs compared to DMSO controls, including a total of 6,550 drugs and 881 cell lines. Considering the available drug data for MM cell lines, we excluded drugs without data for MM cell lines, resulting in a dataset of 639 drugs with data for 16 MM cell lines. The gene expression data for MM cell lines were also acquired from the DepMap website, with data available for 15 of the 16 MM cell lines. We calculated the risk score for each MM cell line. Subsequently, we correlated the risk scores with the fold change data of the drugs, and used the 'EnhancedVolcano' package to create a volcano plot. The top five related drugs were labeled in the volcano plot.

We obtained the RNAi dependency score data, which were already integrated from the Broad Institute Project Achilles, Novartis Project DRIVE, and Marcotte et al., and calculated using the DEMETER2 model [23]. We selected the dependency score data for MM cell lines and performed correlation analysis with the risk score, following the same methodology as the drug analysis. This process allowed us to identify genes whose knockdown significantly decreased the proliferation of high-risk MM cell lines while having less effect on low-risk MM cell lines. We then returned to the MM patient cohort to validate these genes. We correlated the risk score with the transcriptome levels of these genes across four cohorts (MMRF-CoMMpass, GSE136337, GSE24080, and GSE19784). GSE57317 was excluded due to the low sample count. Next, we identified genes that were significantly positively associated across all four cohorts and intersected these with genes that were significantly negatively associated in the RNAi data.

Combining ISS with m6A-related signature

We conducted a multivariate Cox regression analysis incorporating the m6A risk stratification model and other clinical information of MM patients to determine whether the m6A risk stratification serves as an independent prognostic factor. We aimed to integrate the m6A risk stratification system with the International Staging System (ISS) to develop a more precise prognostic stratification system. Given that all arrays, except for the smaller GSE57317 cohort, included ISS scoring data, we combined the m6A pairing model with ISS in a larger sample setting to create a modified ISS. The concordance index (C-index) was used to evaluate and compare the performance of the modified ISS with other models.

Statistical analysis

All statistical analyses in this study were conducted using R software (version 4.3.0). Wilcoxon rank-sum test and Kruskal–Wallis test were applied for the comparison of continuous variables between two or more groups. All figures in this study were generated using the 'ggplot2' package. The analysis of Kaplan–Meier survival curves and Cox regression was conducted using the 'survival' and 'survminer' packages, respectively. For the LASSO regression, we employed the 'glmnet' package. To combine the c-index effect sizes from various arrays, the 'meta' package was used with a random effects model. The log-rank test was applied to calculate p-values for survival analysis, with statistical significance set at $P < 0.05$.

Results

Construction and evaluation of the m6A signature

In our study, we collected data from 2080 patients with multiple myeloma (MM) and their corresponding survival data to develop and validate prognostic models. The MMRF-CoMMpass dataset, with its robust sample size, was designated as the training set. Out of 27 m6A regulatory genes, 13 were found to be significantly associated with prognosis, including CPSF6, FMR1, FTO, HNRNPA2B1, HNRNPC, IGF2BP2, METTL14, NUDT21, RBM15, SRSF10, YTHDF1, YTHDF2, and YTHDF3 (supplementary Table 5). These 13 genes were paired with other available genes to obtain 13*11,769 gene-pairs. Following the filtering steps outlined in the methods section and refinement using nested Cox LASSO regression, a prognostic model with 38 gene-pairs was constructed (Fig. 1a-b). The gene-pairs and their corresponding coefficients are listed in Supplementary Table 6. The risk score for each MM sample was calculated. In the training cohort, an optimal cutoff point

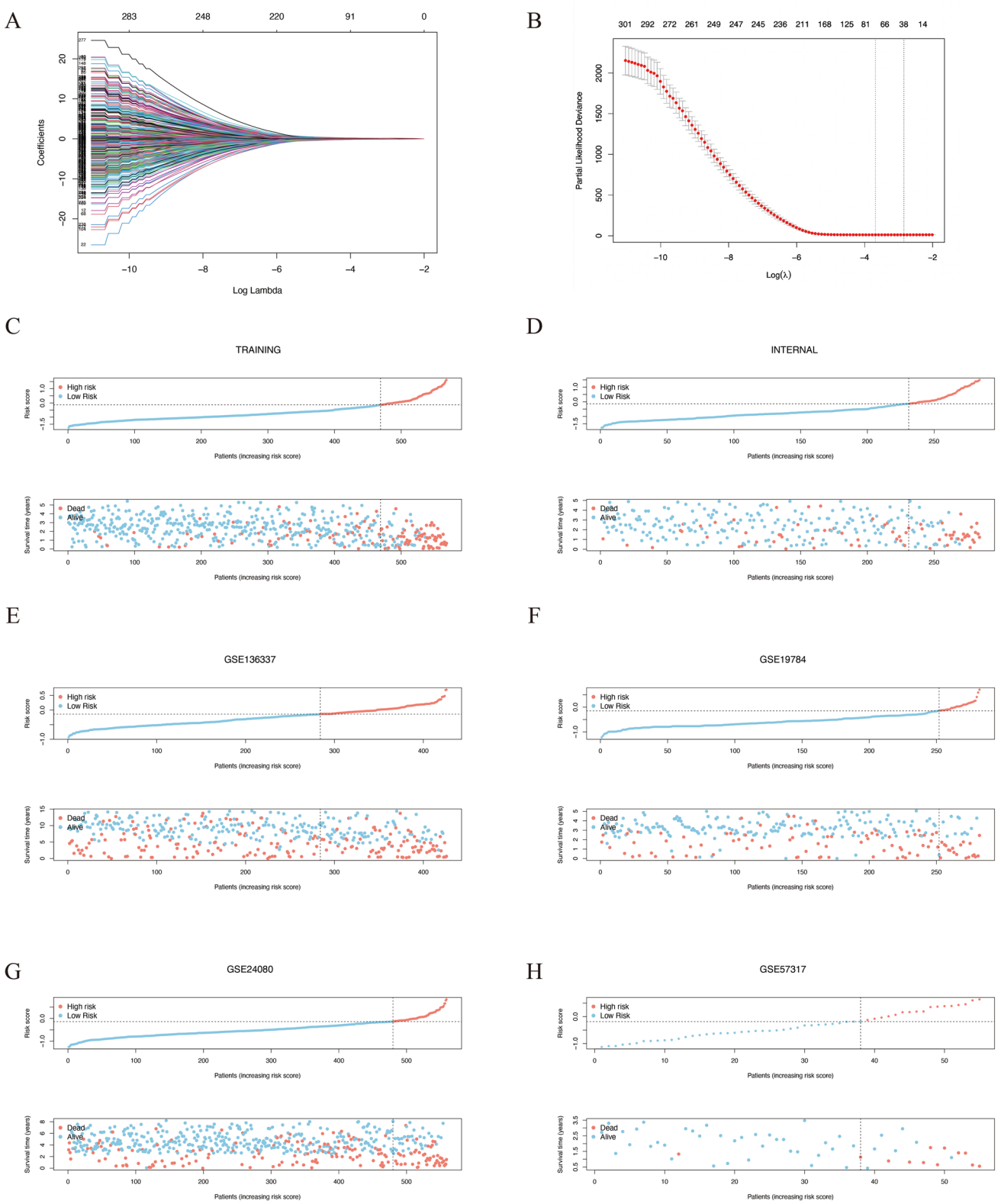

Fig. 1 Development of the m6A gene-pairing model. (**A-B**) In the course of LASSO regression, the increase in penalty coefficients eliminates many gene-pairs' coefficients, while the partial likelihood variation simultaneously decreases, reaching a minimum with a refined set of 38 gene-pairs. (**C-H**) Distribution of risk scores and associated trends in survival status and duration among MM samples with increasing risk scores. The designations of the respective arrays are indicated at the top of each panel

of -0.133 was identified, which significantly distinguished between the high-risk and low-risk groups. This cutoff was also applied to define the high-risk group in both the internal and external test cohorts (Fig. 1c-h).

The variation in the range of risk scores for a risk model across cohorts indicates its stability in response to confounding factors such as batch effects. We created density plots for the m6A risk scores across different cohorts and compared them with other models, using the ISS as a reference. We found that the risk score distribution of the m6A risk model was highly consistent across the five datasets, whereas the other models [26–28] showed significant variation among cohorts (Fig. 2a). Therefore, our gene-pair model is much more stable than the others.

Comparing the KM survival curve of high-risk MM samples with low-risk samples, the high-risk MM samples showed significantly shorter overall survival times than the low-risk samples across both the training and validation cohorts (Fig. 2b). We aimed to determine whether m6A risk stratification is an independent prognostic factor. To do this, we combined m6A risk stratification with other clinical indices such as age, gender, and ISS stage. These variables were included in a multivariate Cox regression analysis across four cohorts with sufficient clinical data, including GSE136337, GSE19784, GSE24080, and MMRFtumor. The results, consistent across all four cohorts, showed that a high m6A risk, with an HR significantly greater than 1 when compared to the low-risk group, remained an independent prognostic factor even when adjusted for other clinical features (Fig. 3). Therefore, m6A risk stratification can independently predict prognosis.

The prognostic impact of factors on MM outcomes may vary across treatment regimens. To assess the predictive performance of the m6A risk score across different treatment settings, we compared C-index values within various therapeutic groups. First, in the MMRFtumor cohort, we compared samples with 1 autologous stem cell transplant to those without any transplant. To control for drug treatment effects, we focused on MM samples treated with a regimen comprising immunomodulatory agents, proteasome inhibitors, corticosteroids, and alkylating agents, as this was the most prevalent treatment group. Additionally, due to the small number of samples with more than one transplant, we excluded this group from the analysis. The results showed no significant difference in C-index between the 1-transplant and 0-transplant groups (Fig. 4a). Using clinical data from the GSE136337 cohort, we further compared C-index values for MM samples that had undergone more than 2 stem cell transplants versus those with 2 or fewer. Results demonstrated a slight increase in the C-index for the group with 2 or fewer transplants, though confidence intervals overlapped (Fig. 4a). We also analyzed treatment regimen data from the MMRFtumor cohort, excluding groups with fewer than 50 samples, and classified the remaining samples into three treatment regimen groups for comparison (restricted to MM samples without stem cell transplants). Regimen (1) included immunomodulatory agents, proteasome inhibitors, and corticosteroids; Regimen (2) consisted of proteasome inhibitors, corticosteroids, and alkylating agents; and Regimen (3) comprised immunomodulatory agents, proteasome inhibitors, corticosteroids, and alkylating agents. The results indicated an upward trend in the C-index for Regimens 1 and 3 compared to Regimen 2 (Fig. 4b). Given that the absence of immunomodulatory agents was the key distinction in Regimen 2, we hypothesized that the m6A risk score might perform better in samples treated with immunomodulatory agents. To test this, we stratified samples based on immunomodulatory agent use and conducted C-index analysis, observing an upward trend in the C-index among samples that received immunomodulatory agents (Fig. 4b). In summary, while no statistically significant differences were observed, the m6A risk score demonstrated improved predictive performance in MM samples that received immunomodulatory agents or had undergone 2 or fewer transplants.

m6A risk score as a predictor of MM therapy response

The results have shown that m6A risk stratification is an independent prognostic factor, so determining whether this risk model can predict the response to MM therapy is important. We identified an MM cohort containing refractory MM samples with single-cell data that failed to respond to initial bortezomib-based induction. A DARA-KRD regimen, including monoclonal antibodies, proteasome inhibitors, immunomodulators, and glucocorticoids, was administered to these refractory MM patients. By correlating the therapy data with the m6A risk score, we found that the non-responder group had significantly higher m6A risk scores than the responder group (Fig. 5a) ($p < 0.001$). The ROC curve was used to evaluate the ability of the m6A risk score to distinguish therapy response, yielding an AUC value of 90% (Fig. 5a). According to this evidence, the m6A risk score can accurately predict MM therapy response, which may explain its role as an independent prognostic factor.

m6A risk score as a marker of MM progression

We integrated data from seven different arrays to compare the m6A risk scores across various stages of MM progression. We found that m6A risk scores increased progressively from healthy controls to MGUS, SMM, MM, relapsed MM, and PCL (Fig. 5b). The ability of m6A risk scores to distinguish between these stages was assessed by comparing the AUC values between pairs of stages. Except for the

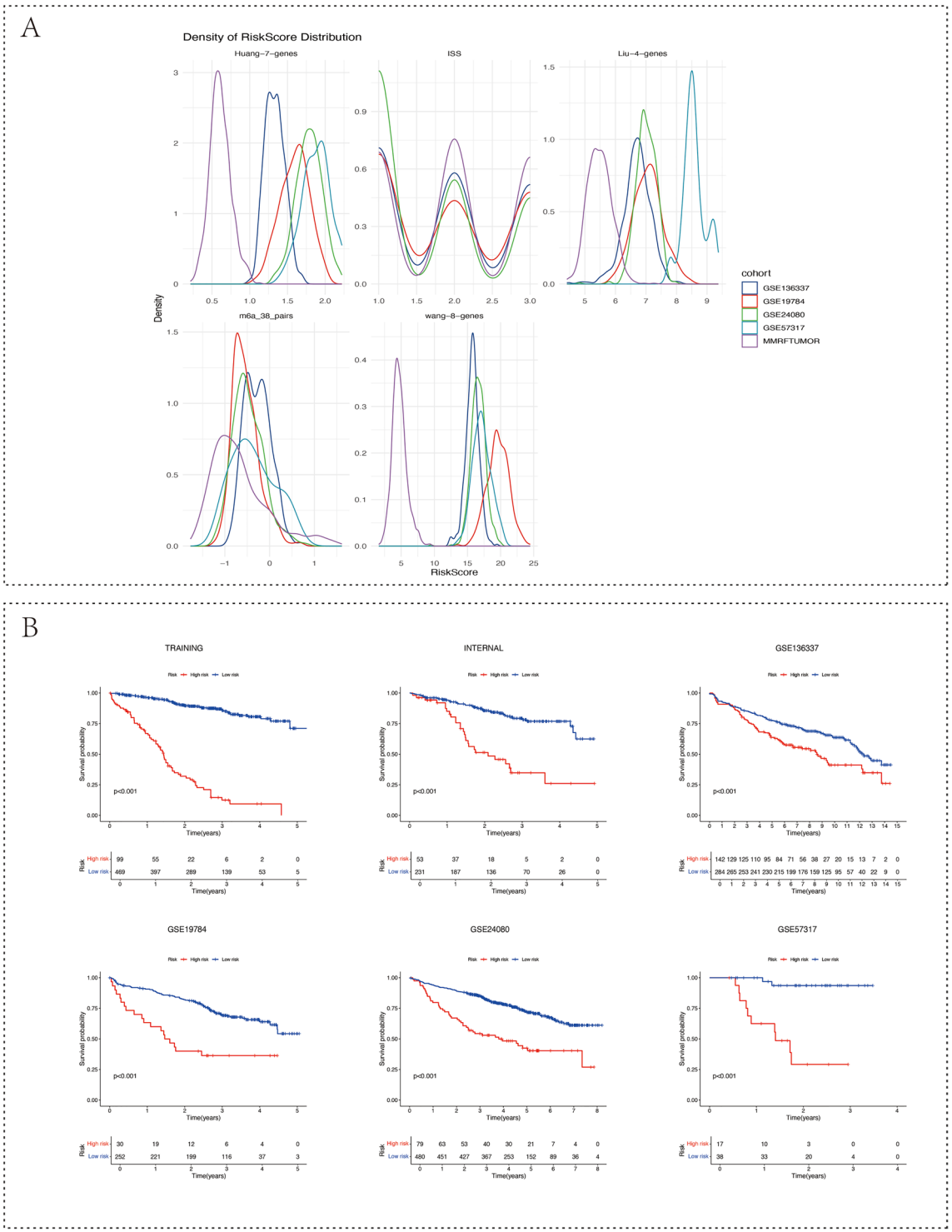

Fig. 2 Kaplan–Meier survival curves and distribution of m6A risk scores. (**A**) Comparison of the m6A 38-pair model with ISS and other gene expression-based prognostic models. Different colors represent different arrays. (**B**) These six Kaplan–Meier plots display the differences in overall survival between high-risk and low-risk groups stratified by the m6A pairing model across various datasets. High-risk groups are shown in red, while low-risk groups are depicted in blue

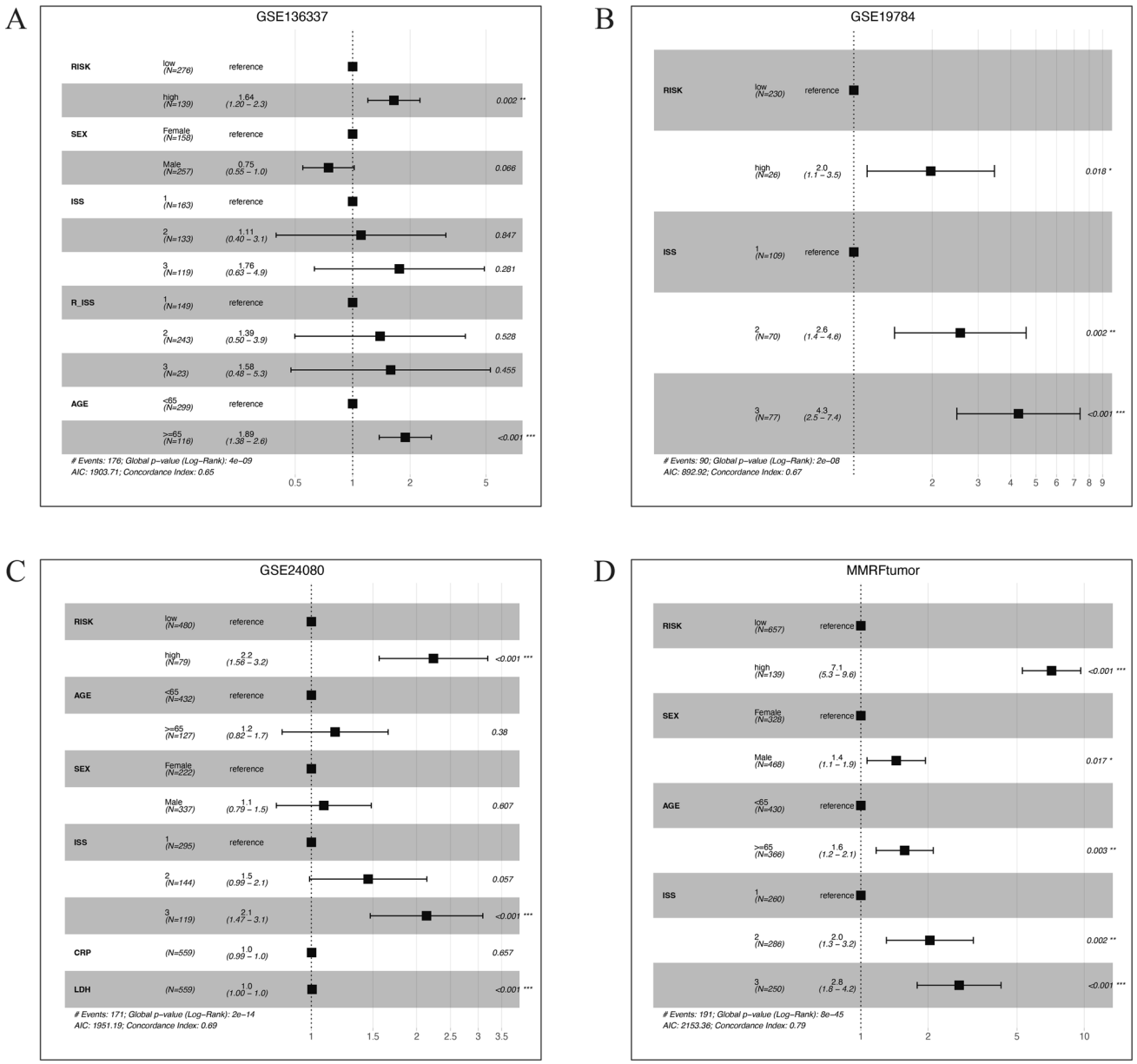

Fig. 3 m6A risk model as an independent prognostic factor. Forest plots in panels A-D illustrate multivariate Cox regression analyses across four different datasets, each indicated at the top of the plot. The 'RISK' label corresponds to the m6A risk model in the first column of the forest plot, showing that in each scenario, the high-risk group has a hazard ratio (HR) significantly higher than one compared to the low-risk group

relatively low discriminatory power between healthy controls, MGUS, and SMM, the AUC values between other stages were all above 0.6 (Fig. 5c). Notably, although SMM and MM exhibit high genomic similarity [29], m6A risk scores effectively distinguished between them (AUC = 0.76). The m6A risk score also accurately differentiated between plasma cell leukemia (PCL) and MM (AUC = 0.81). Additionally, we calculated the optimal cutoff values for distinguishing between paired stages using the Youden index, with -0.45 for MM and SMM, and 0.0857 for MM and PCL (Supplementary Table 7). This evidence suggests that m6A risk scores reflect the intrinsic malignant progression of tumor samples, which may be an underlying reason why a high m6A risk score corresponds to poorer prognosis.

The m6A risk scores upregulated at MM relapse

Clonal evolution of tumor clones occurs in response to therapeutic pressure, and it has been established that m6A modifications play a role in therapy resistance in multiple myeloma

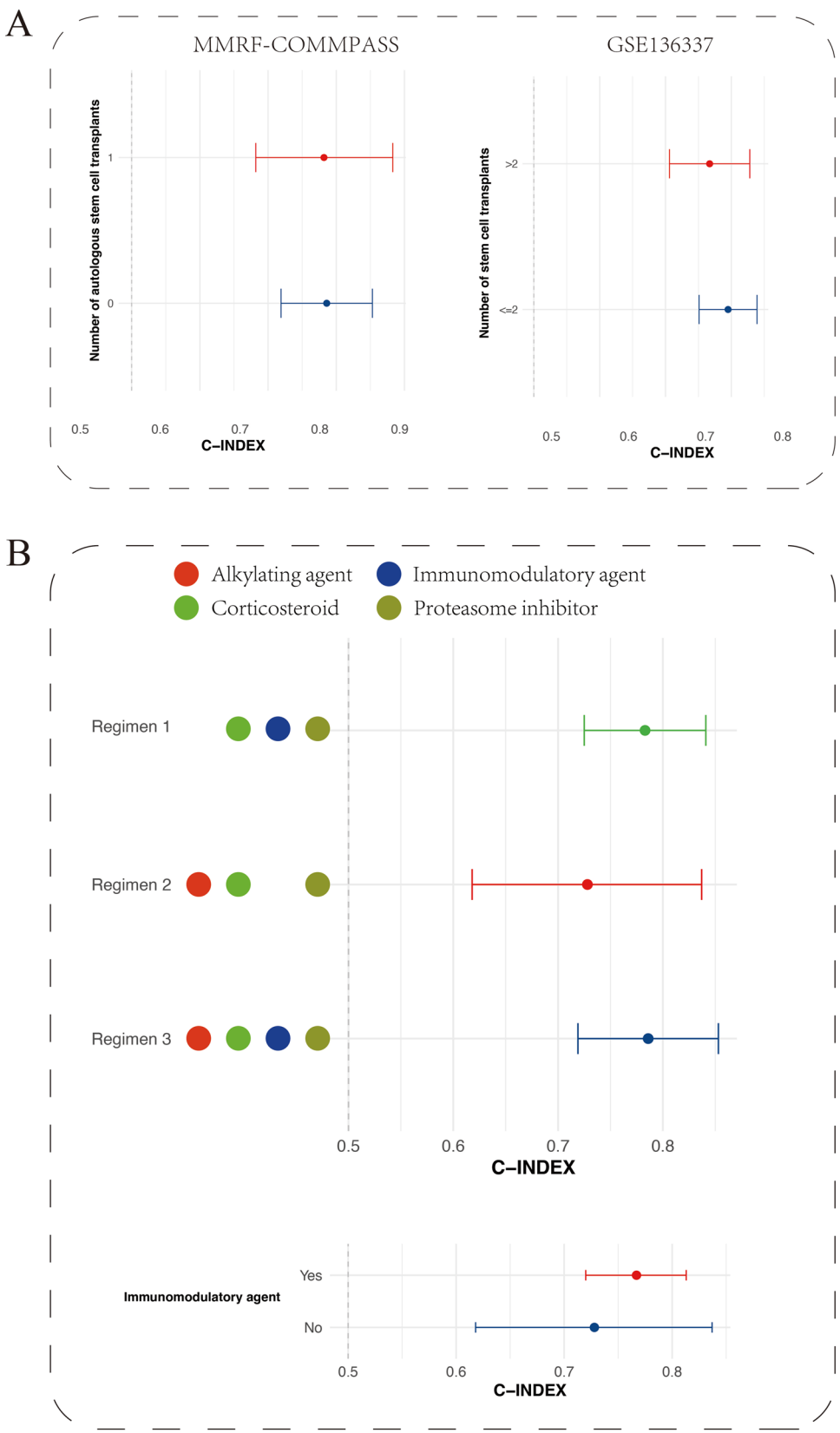

Fig. 4 Comparison of C-index for m6A risk scores across different treatment groups. (**A**) Forest plots depicting the C-index based on the number of stem cell transplants. The left panel presents data from the MMRF-COMMPASS cohort, with the y-axis indicating autologous stem cell transplant status (0 or 1 transplant); the right panel shows results from the GSE136337 cohort, with the y-axis indicating whether patients received more than 2 transplants or 2 or fewer. The x-axis in both panels represents the C-index. (**B**) In the upper forest plot, the C-index and corresponding confidence intervals are shown for three distinct treatment regimens. The lower forest plot illustrates the C-index and confidence intervals for groups stratified by the use of immunomodulatory agents

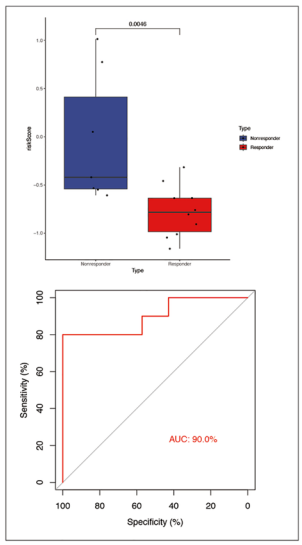
A
0.0046
riskScore
Type
Nonresponder
Responder
Sensitivity (%)
Specificity (%)
AUC: 90.0%

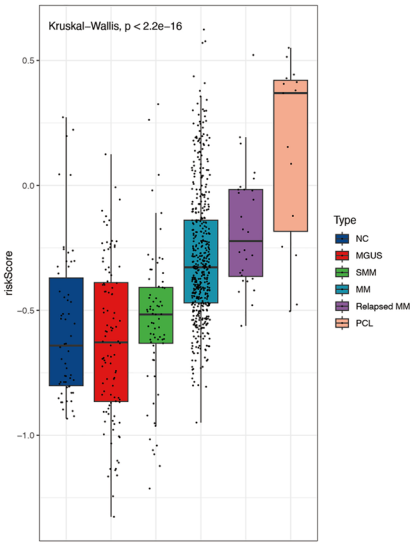
B
Kruskal–Wallis, p < 2.2e−16
riskScore
Type
NC
MGUS
SMM
MM
Relapsed MM
PCL

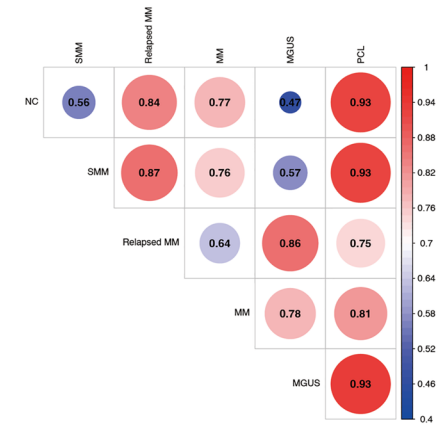
C
SMM
Relapsed MM
MM
MGUS
PCL
NC
0.56
0.84
0.77
0.47
0.93
SMM
0.87
0.76
0.57
0.93
Relapsed MM
0.64
0.86
0.75
MM
0.78
0.81
MGUS
0.93

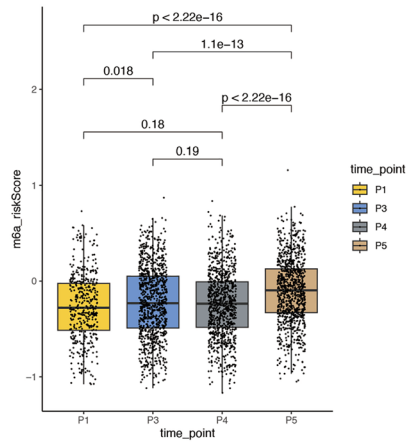
D
p < 2.22e−16
1.1e−13
0.018
p < 2.22e−16
0.18
0.19
m6a_riskScore
time_point
P1
P3
P4
P5

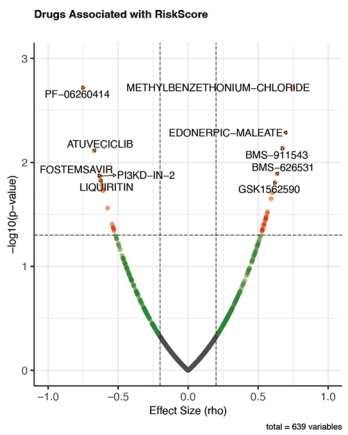
E
Drugs Associated with RiskScore
PF−06260414
METHYLBENZETHONIUM−CHLORIDE
ATUVECICLIB
EDONERPIC−MALEATE
BMS−911543
FOSTEMSAVIR
PI3KD−IN−2
BMS−626531
LIQUIRITIN
GSK1562590
−log10(p−value)
Effect Size (rho)
total = 639 variables

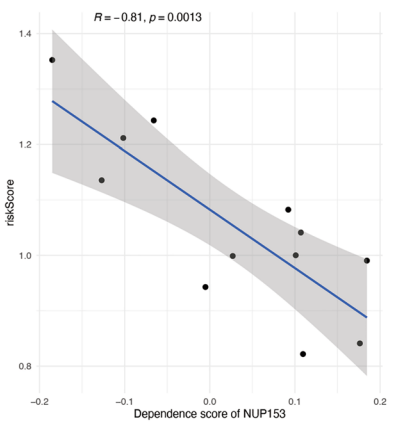
F
R = −0.81, p = 0.0013
riskScore
Dependence score of NUP153

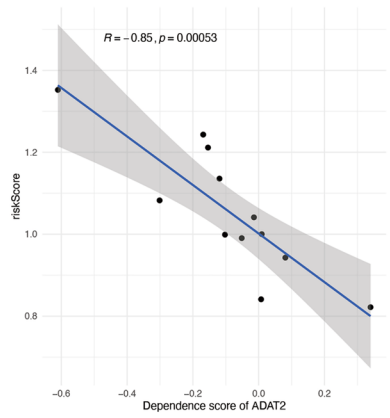
G
R = −0.85, p = 0.00053
riskScore
Dependence score of ADAT2

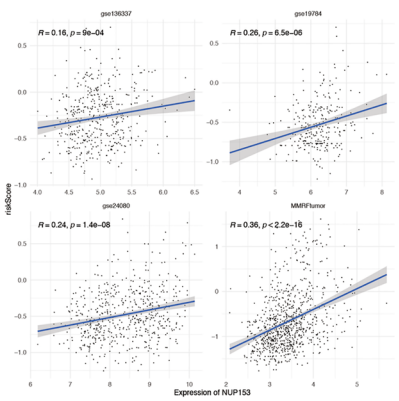
H
gse136337
R = 0.16, p = 9e−04
gse19784
R = 0.26, p = 6.5e−06
gse24080
MM/FUmor
R = 0.24, p = 1.4e−08
R = 0.36, p < 2.2e−16
riskScore
Expression of NUP153

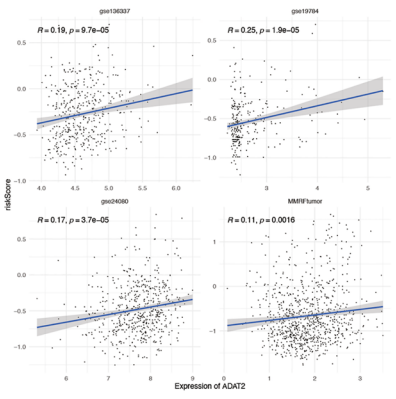
I
gse136337
R = 0.19, p = 9.7e−05
gse19784
R = 0.25, p = 1.9e−05
gse24080
MM/FUmor
R = 0.17, p = 3.7e−05
R = 0.11, p = 0.0016
riskScore
Expression of ADAT2

◂**Fig. 5** The m6A risk score is significantly associated with MM treatment response, malignancy, and relapse. (**A**) The upper box plot shows that the m6A risk score is significantly higher in the non-responsive group compared to the responsive group following MM treatment. The lower ROC plot evaluates the m6A risk score's ability to distinguish between different treatment response groups, with an AUC of 90%. (**B**) Six box plots illustrate m6A risk scores in samples from six stages of MM progression: normal controls (NC), monoclonal gammopathy of undetermined significance (MGUS), smoldering multiple myeloma (SMM), multiple myeloma (MM), relapsed MM, and plasma cell leukemia (PCL). (**C**) The heatmap displays the AUC values of m6A risk scores in distinguishing between these stages, with red indicating higher AUC values and blue indicating lower values. (**D**) Four box plots compare the distribution of m6A risk scores in samples from a single MM patient at four different time points: P1 represents the initial diagnosis sample; P3, the sample after relapse following lenalidomide treatment; P4, the sample after relapse following lenalidomide and ixazomib treatment; and P5, the sample after relapse following daratumumab and bortezomib treatment. The samples follow a chronological order from P1 to P5, with P1 being the earliest and P5 the latest, indicating multiple relapses. The risk scores for P3 and P5 are significantly higher compared to P1. (**E**) The volcano plot shows the correlation between m6A risk scores and drug sensitivity across 15 MM cell lines, with the x-axis representing the correlation coefficient and the y-axis representing -log10(p value). The top five most correlated drugs are labeled on the plot. (F-G) Correlation analysis results between the dependence scores of NUP153 and ADAT2 and m6A risk scores in MM cell lines, showing significant negative correlations. (H-I) Correlation analysis results between the gene expression of NUP153 and ADAT2 and m6A risk scores in multiple MM sample arrays, showing significant positive correlations

(MM). We aimed to investigate whether m6A risk scores change from initial diagnosis to relapse. In a non-paired differential analysis of m6A risk scores between newly diagnosed MM samples and relapse MM samples from the merged datasets mentioned in Sect. "m6A risk score as a marker of MM progression," we observed a significant upregulation of m6A risk scores in the relapse group.

Additionally, we analyzed the risk score changes over multiple time points in a single MM patient from the GSE161195 dataset. This patient had samples collected at four time points: initial diagnosis (P1), relapse after lenalidomide treatment (P3), relapse after lenalidomide and ixazomib treatment (P4), and relapse after daratumumab and bortezomib treatment (P5). Comparing the distribution of risk scores across these time points, we found that the scores in P3 and P5 were upregulated compared to P1, with the highest risk score observed at P5 (Fig. 5d). Furthermore, in another subset of the GSE161195 dataset containing pair-wise single-cell data before and after therapy, we utilized the pair-wise Wilcoxon test to compare m6A risk scores between baseline and after cycle 4 or cycle 10 of the DARA-KRD regimen. The results showed a significant increase in risk scores after both cycle 4 and cycle 10 compared to baseline, but no significant difference between cycle 4 and cycle 10 (Supplementary Fig. 2). These findings collectively indicate that m6A risk scores are upregulated at MM relapse.

Identifying potential drugs and targets for the m6A high-risk group

The m6A risk model categorizes MM patients into high-risk and low-risk groups, prompting us to identify drugs with enhanced sensitivity in the high-risk group. Using the PRISM Repurposing Public 23Q2 drug sensitivity data, we analyzed the correlation between the m6A risk scores of 15 MM cell lines and the logFC values (fold change in cell number compared to control after 5 days of treatment at 2 μM concentration) of 639 drugs. We identified 14 drugs that were significantly negatively correlated with the risk scores (Fig. 5e). The five drugs with the strongest negative correlation were atuveciclib (CDK9 inhibitor), fostemsavir (antiviral), PI3KD-IN-2 (PI3K inhibitor), PF-06260414 (androgen receptor modulator), and liquiritin (antioxidant). These potential drugs demonstrated stronger sensitivity in the high-risk group, suggesting their potential efficacy.

In addition to identifying drugs, we aimed to discover potential therapeutic targets for the m6A high-risk group. Using RNAi data from DepMap, we calculated the correlation between the m6A risk scores of 16 MM cell lines and the dependence scores of 11,096 genes. (Lower scores indicate greater impairment of cell proliferation upon gene knockdown.) We identified 38 genes with a correlation coefficient less than −0.7, indicating that knocking down these genes significantly impacts the proliferation of MM cell lines in the high-risk group (Supplementary Table 8). This suggests a mutual exclusivity between low expression of these genes and high m6A risk scores. To validate this mutual exclusivity, we analyzed the correlation between m6A risk scores and the expression of these genes using MM sample data from four arrays (GSE13667, GSE24080, GSE19784, and MMRFtumor). Interestingly, we found that the expression of two genes, ADAT2 and NUP153, was significantly positively correlated with the risk scores across all four arrays (Fig. 5f-i). Based on this evidence, inhibiting the function or expression of ADAT2 and NUP153 is likely to suppress the growth of cancer cells in high-risk MM samples.

Integrating ISS with the m6A model

With ISS data available in four datasets (GSE136337, GSE19784, GSE24080, MMRF tumor), covering a total of 2026 samples, we stratified MM patients into six novel categories based on ISS and m6A risk scores (Fig. 6a). Within these six groups, samples with ISS stage 2 and high m6A risk scores exhibited poorer prognoses compared to those with ISS stage 3 and low m6A risk scores. Consequently, we defined groups 3-high, 3-low, and 2-high as the high-risk category. Samples with ISS stage 1 and high m6A risk scores had overall survival rates similar to those with ISS stage 2

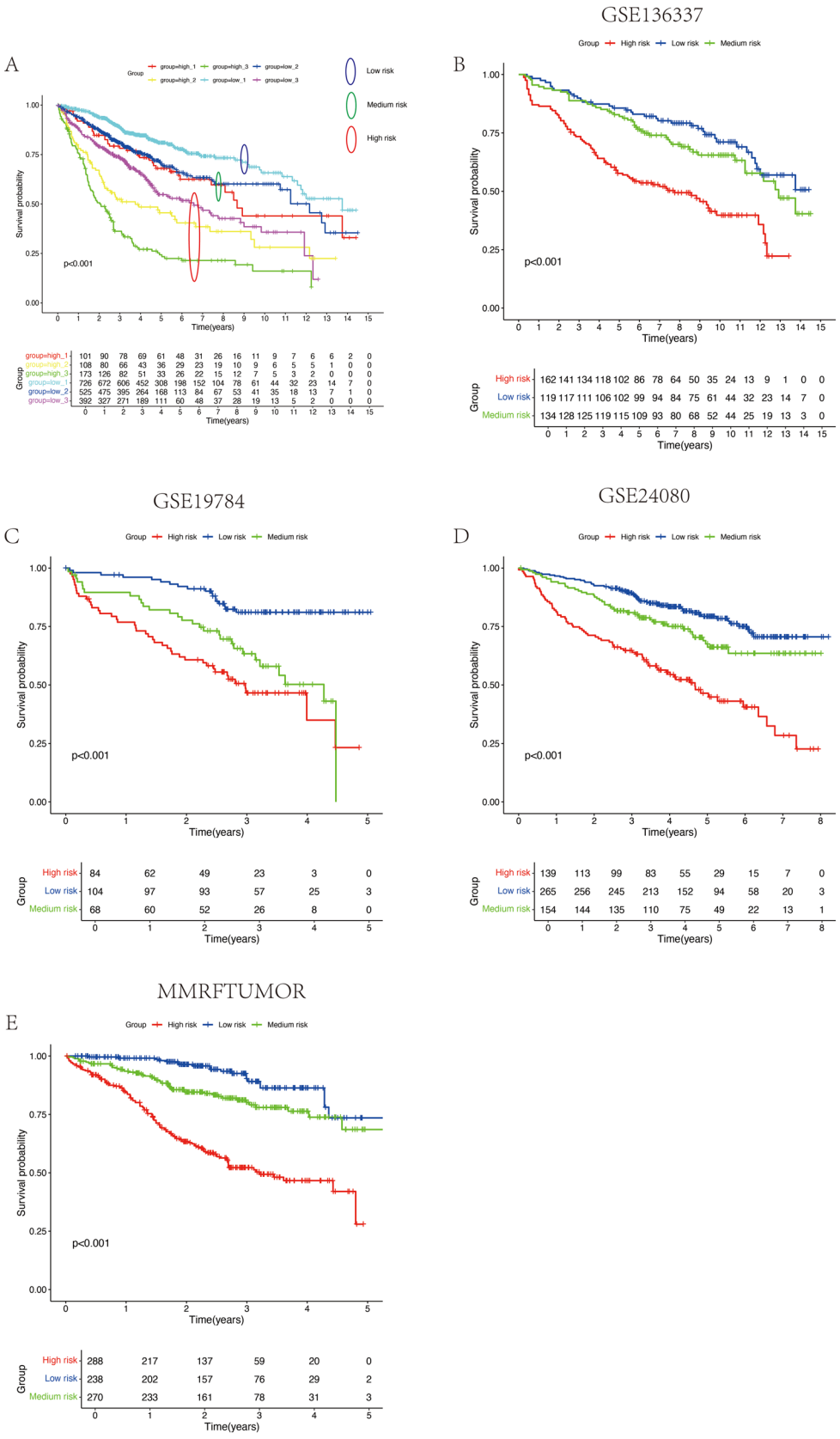

Fig. 6 Combining the m6A risk model with ISS to form m6A-enhanced ISS categories. (**A**) Overall survival comparison across six MM sample cohorts within the combined dataset, with ellipses indicating the reclassification method. (**B-E**) Survival comparisons among m6A-enhanced ISS categories across four distinct datasets

and low m6A risk scores, both significantly shorter than those in group 1-low. Thus, we classified groups 2-low and 1-high as the intermediate-risk category, and group 1-low as the low-risk category. This new stratification method was termed the m6A-enhanced ISS (Table 1). To evaluate the prognostic performance of the m6A-enhanced ISS, we first used Kaplan–Meier (KM) curves to compare overall survival (OS) among high-, medium-, and low-risk groups across four datasets (GSE136337, GSE19784, GSE24080, MMRF tumor) (Figs. 6b-e). The results revealed significant differences in OS among the three groups, with the high-risk group exhibiting the shortest survival, followed by the medium-risk group, and then the low-risk group. Additionally, to compare the predictive performance of the m6A-enhanced ISS with other models, we calculated the concordance index (C-index) for each model within each MM sample array. In the arrays where the m6A-enhanced ISS model could be applied, the C-index of the m6A-enhanced ISS was significantly higher than that of other models, except in GSE19784, where the C-index was slightly lower than that of the ISS. Furthermore, in GSE136337, the C-index of the m6A-enhanced ISS was significantly higher than that of the R-ISS (Fig. 7). To integrate the results from all available arrays, we performed a meta-analysis of the C-index using a random effects model. According to the integrated C-index results, the m6A-enhanced ISS exhibited the best predictive performance, followed by the ISS, the m6A prognostic model, and the R-ISS (Fig. 7, META section lower right). These findings highlight the superior prognostic accuracy of the m6A-enhanced ISS over the conventional ISS and R-ISS.

Discussion

In this study, we developed an m6A gene-pairing risk stratification model using transcriptomic data from previously reported m6A regulatory genes. Using a cutoff of -0.133, we categorized MM samples into high-risk and low-risk groups. The high-risk group exhibited significantly poorer prognosis, and multivariate Cox regression analysis confirmed that the m6A risk stratification model is an independent prognostic factor. Furthermore, we found that the m6A risk score could accurately predict MM treatment responses, with significantly elevated risk scores in the non-responsive group. This finding partially explains why the m6A risk model is an independent prognostic factor across multiple datasets, as it relates to treatment response.

Subsequently, we analyzed the m6A risk scores at different stages of MM progression. The results indicated that the risk scores significantly increased with the malignancy of MM, reaching the highest levels at the PCL stage. Additionally, the risk score had an AUC of 0.76 in distinguishing SMM from MM, indicating that the m6A risk score can effectively differentiate between SMM and MM. Current studies suggest that SMM and MM share similar genomic characteristics, including clonal heterogeneity and gene mutation landscapes [30]. This suggests that an epigenetic perspective, such as examining m6A modifications, may offer a novel approach for exploring the differences between SMM and MM and for determining which subset of SMM patients might benefit from early intervention. Furthermore, the m6A risk score can effectively distinguish between MM and PCL, with an AUC of 0.81. This evidence underscores the significant association between the m6A risk score and the malignancy of MM, thereby validating the effectiveness of the m6A risk model.

We also analyzed the changes in m6A risk scores in MM samples upon relapse, and the results indicated that the risk scores were significantly higher in relapse samples compared to initial diagnosis samples. In a patient with multiple relapses, the risk score at the last relapse was significantly higher than at the first relapse. This suggests clonal evolution in MM under treatment pressure, where resistant clones exhibit higher risk scores. This finding aligns with the observation that the risk score can predict treatment response, indicating that the m6A risk score may quantify the resistance characteristics of MM samples and further validating the feasibility of the m6A risk model.

We integrated the m6A risk model with the International Staging System (ISS) to create an m6A-refined ISS risk model, which significantly enhanced the risk stratification capability of the ISS. In the GSE136337 dataset, the m6A-refined ISS outperformed the Revised ISS (R-ISS). Our m6A risk model was constructed using a gene-pairing approach, minimizing the impact of batch effects and differences in measurement methods. Our results confirmed this, as the distribution of m6A risk scores across different datasets showed significantly less variability compared to other non-gene-pairing models. The model demonstrated usability across various measurement platforms, including microarray data, next-generation sequencing, and UMI-based single-cell transcriptome sequencing data (single-cell or pseudobulk data).

Table 1 Refined new ISS re-categorization based on m6A risk and ISS

m6A risk group	ISS	m6A-enhanced ISS
low	1	low
low	2	medium
high	1	medium
low	3	high
high	2	high
high	3	high

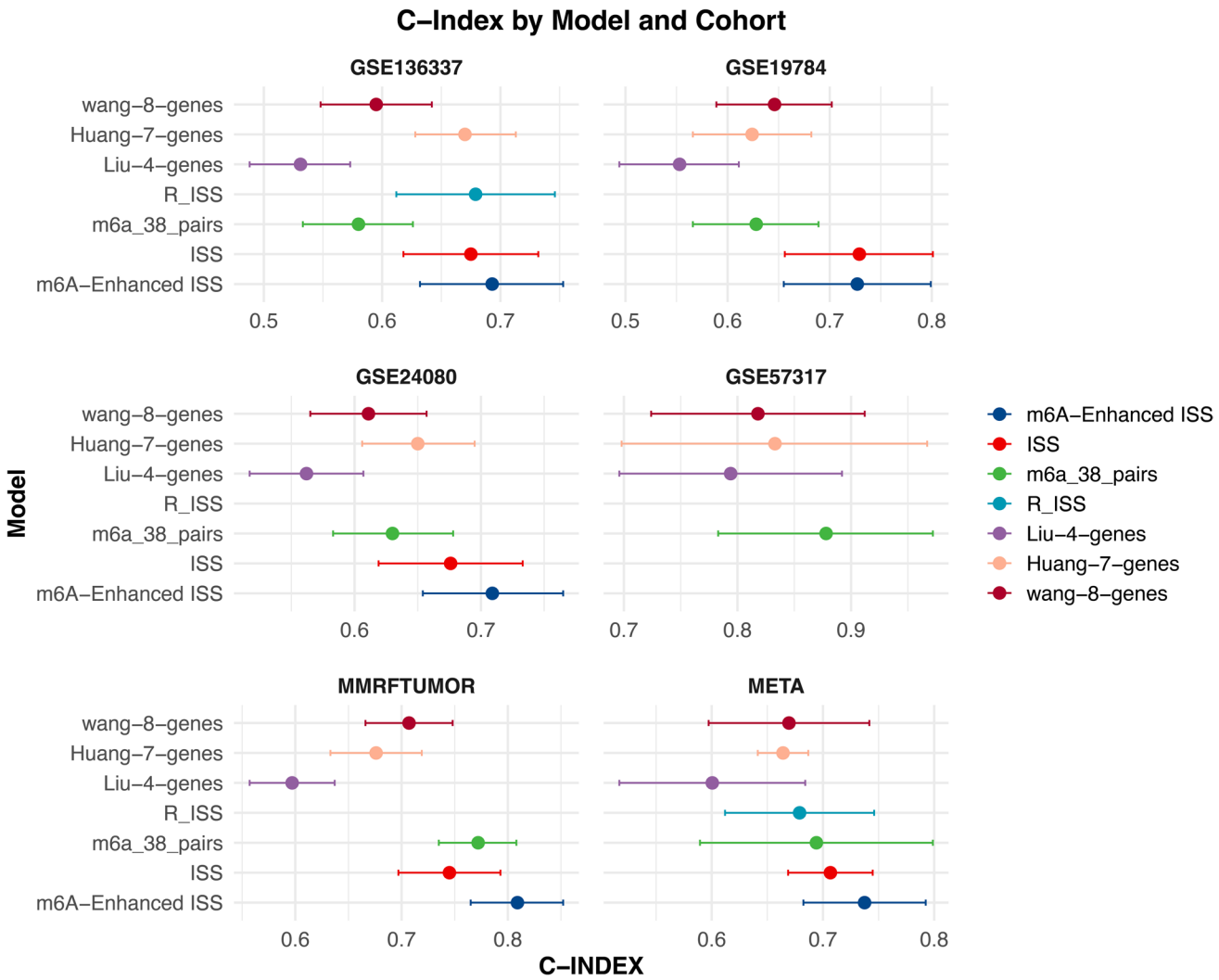

Fig. 7 Evaluation of prognostic performance across models. The C-index is used to measure predictive performance, with the first plot showing the 95% confidence intervals of the indices. The diagram is divided into six sections: The first five correspond to individual datasets, while the final section summarizes findings from the meta-analysis of the combined datasets

However, our study has some limitations. First, due to the availability of datasets containing R-ISS data, we could only demonstrate the superiority of the m6A-refined ISS over the R-ISS in one dataset. More subsequent studies are needed to objectively evaluate the advantages of the m6A-refined ISS compared to the R-ISS. Additionally, while we identified some potential drugs and targets for the high-risk group through bioinformatic analysis, clinical trials are needed to validate these findings.

In summary, we have developed an m6A prognostic model that can accurately predict prognosis and treatment response, describe the malignancy and resistance characteristics of MM, and enhance risk stratification when combined with the ISS to form the m6A-refined ISS. This provides a new strategy for the precision treatment of MM.

Supplementary Information The online version contains supplementary material available at https://doi.org/10.1007/s10238-024-01526-6.

Acknowledgements Appreciating the computing resources provided by the high-performance computing service platform of Central South University.

Author contributions H.P. designed and composed the study. Y.D. collected the data, conducted the bioinformatics analysis, and composed the manuscript. H.Z. assisted with the interpretation of the data. All authors reviewed and approved the final manuscript.

Funding This work was supported by the National Natural Science Foundation of China (82070175) and the Scientific program of Health Commission of Hunan Province (20201179).

Data availability No datasets were generated or analyzed during the current study.

Declarations

Conflict of interest The authors declare no competing interests.

Consent for publication Not applicable.

Ethics approval Not applicable.

References

1. Gerecke C, et al. The diagnosis and treatment of multiple myeloma. Deutsch Arztebl Int. 2016;113:470–6.
2. Palumbo A, Anderson K. Multiple myeloma. N Engl J Med. 2011;364:1046–60.
3. Kyle RA, et al. A long-term study of prognosis in monoclonal gammopathy of undetermined significance. N Engl J Med. 2002;346:564–9.
4. Prideaux SM, O'Brien EC, Chevassut TJ. The genetic architecture of multiple myeloma. Adv Hematol. 2014;2014:1–16. https://doi.org/10.1155/2014/864058.
5. Greipp PR, et al. International staging system for multiple myeloma. J Clin Oncol. 2005;23:3412–20.
6. Palumbo A, et al. Revised international staging system for multiple myeloma: a report from international myeloma working group. J Clin Oncol. 2015;33:2863–9.
7. Szalat R, Avet-Loiseau H, Munshi NC. Gene expression profiles in myeloma: ready for the real world? Clin Cancer Res. 2016;22:5434–42.
8. Kong W, et al. An immunity and pyroptosis gene-pair signature predicts overall survival in acute myeloid leukemia. Leukemia. 2022;36:2384–95.
9. Jiang F, et al. HNRNPA2B1 promotes multiple myeloma progression by increasing AKT3 expression via m6A-dependent stabilization of ILF3 mRNA. J Hematol Oncol. 2021;14:54.
10. Jia C, et al. HNRNPA2B1-mediated m6A modification of TLR4 mRNA promotes progression of multiple myeloma. J Transl Med. 2022;20:537.
11. Xu A, et al. FTO promotes multiple myeloma progression by posttranscriptional activation of HSF1 in an m(6)A-YTHDF2-dependent manner. Mol Ther. 2022;30:1104–18.
12. Song S, et al. IDH2 contributes to tumorigenesis and poor prognosis by regulating m6A RNA methylation in multiple myeloma. Oncogene. 2021;40:5393–402.
13. Liu R, et al. N6-methyladenosine reader YTHDF2 promotes multiple myeloma cell proliferation through EGR1/p21(cip1/waf1)/CDK2-Cyclin E1 axis-mediated cell cycle transition. Oncogene. 2023;42:1607–19.
14. Hua Z, et al. YTHDF2 promotes multiple myeloma cell proliferation via STAT5A/MAP2K2/p-ERK axis. Oncogene. 2022;41:1482–91.
15. Che F, et al. METTL3 facilitates multiple myeloma tumorigenesis by enhancing YY1 stability and pri-microRNA-27 maturation in m(6)A-dependent manner. Cell Biol Toxicol. 2023;39:2033–50.
16. Yu T, et al. ALKBH5 Promotes Multiple Myeloma Tumorigenicity through inducing m(6)A-demethylation of SAV1 mRNA and myeloma stem cell phenotype. Int J Biol Sci. 2022;18:2235–48.
17. He L, et al. Functions of N6-methyladenosine and its role in cancer. Mol Cancer. 2019;18:176.
18. Jiang X, et al. The role of m6A modification in the biological functions and diseases. Signal Transduct Target Ther. 2021;6:74.
19. Sendinc E, Shi Y. RNA m6A methylation across the transcriptome. Mol Cell. 2023;83:428–41.
20. Zhuang H, et al. The role of m6A methylation in therapy resistance in cancer. Mol Cancer. 2023;22:91.
21. Cohen YC, et al. Identification of resistance pathways and therapeutic targets in relapsed multiple myeloma patients through single-cell sequencing. Nat Med. 2021;27:491–503.
22. Masuda T, Haji S, Nakashima Y, Tsuda M, Kimura D, Takamatsu A, Iwahashi N, Umakoshi H, Shiratsuchi M, Kikutake C, Suyama M, Ohkawa Y, Ogawa Y. Identification of a drug-response gene in multiple myeloma through longitudinal single-cell transcriptome sequencing. iScience. 2022;25(8):104781. https://doi.org/10.1016/j.isci.2022.104781.
23. Tsherniak A, et al. Defining a cancer dependency map. Cell. 2017;170:564-576.e516.
24. Tibshirani R. The lasso method for variable selection in the Cox model. Stat Med. 1997;16:385–95.
25. Corsello SM, et al. Discovering the anti-cancer potential of non-oncology drugs by systematic viability profiling. Nat Cancer. 2020;1:235–48.
26. Huang HY, et al. A prognostic survival model based on metabolism-related gene expression in plasma cell myeloma. Leukemia. 2021;35:3212–22.
27. Liu R, et al. Comprehensive analysis of m6A RNA methylation regulators in the prognosis and immune microenvironment of multiple myeloma. Front Oncol. 2021;11:731957.
28. Wang W, et al. Identification and validation of a novel RNA-binding protein-related gene-based prognostic model for multiple myeloma. Front Genet. 2021;12:665173.
29. Walker BA, et al. Intraclonal heterogeneity is a critical early event in the development of myeloma and precedes the development of clinical symptoms. Leukemia. 2014;28:384–90.
30. Mann H, Katiyar V, Varga C, Comenzo RL. Smoldering multiple myeloma - past, present, and future. Blood Rev. 2022;52:100869.

Authors and Affiliations

Yating Deng[1,2,3] · Hongkai Zhu[1,2,3] · Hongling Peng[1,2,3,4]

✉ Hongling Peng
penghongling@csu.edu.cn

[1] Department of Hematology, The Second Xiangya Hospital, Central South University, Changsha 410011, Hunan, People's Republic of China

[2] Institute of Hematology, Central South University, Changsha 410011, Hunan, People's Republic of China

[3] Hunan Engineering Research Center of Cell Immunotherapy for Hematopoietic Malignancies, Changsha 410011, Hunan, People's Republic of China

[4] Hunan Key Laboratory of Tumor Models and Individualized Medicine, Changsha 410011, Hunan, People's Republic of China